THE JOURNAL OF PHYSICAL CHEMISTRY B

Article

pubs.acs.org/JPCB

Shear-Stress-Induced Conformational Changes of von Willebrand Factor in a Water–Glycerol Mixture Observed with Single Molecule Microscopy

Robrecht M. A. Vergauwe,[†] Hiroshi Uji-i,[†] Karen De Ceunynck,[‡] Jan Vermant,[§] Karen Vanhoorelbeke,[‡] and Johan Hofkens*[,†,∥]

[†]Division of Molecular Imaging and Photonics, Department of Chemistry, University of Leuven (KULeuven), Celestijnenlaan 200F, B-3001 Leuven, Belgium

[‡]Laboratory for Thrombosis Research, Interdisciplinary Research Facility Life Sciences, KU Leuven KULAK, Etienne Sabbelaan 53, B-8500 Kortrijk, Belgium

[§]Department of Chemical Engineering, University of Leuven (KULeuven), W. de Croylaan 46, B-3001 Leuven, Belgium

[∥]Nano-Science Center/Department of Chemistry, University of Copenhagen, Universitetsparken 5, 2100 Copenhagen, Denmark

Supporting Information

ABSTRACT: The von Willebrand factor (VWF) is a human plasma protein that plays a key role in the initiation of the formation of thrombi under high shear stress in both normal and pathological situations. It is believed that VWF undergoes a conformational transition from a compacted, globular to an extended form at high shear stress. In this paper, we develop and employ an approach to visualize the large-scale conformation of VWF in a (pressure-driven) Poiseuille flow of water–glycerol buffers with wide-field single molecule fluorescence microscopy as a function of shear stress. Comparison of the imaging results for VWF with the results of a control with λ-phage double-stranded DNA shows that the detection of individual VWF multimers in flow is feasible. A small fraction of VWF multimers are observed as visibly extended along one axis up to lengths of 2.0 μm at high applied shear stresses. The size of this fraction of molecules seems to exhibit an apparent dependency on shear stress. We further demonstrate that the obtained results are independent of the charge of the fluorophore used to label VWF. The obtained results support the hypothesis of the conformational extension of VWF in shear flow.

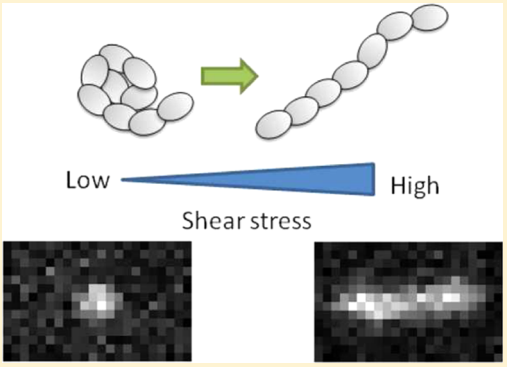

INTRODUCTION

The von Willebrand factor (abbreviated VWF) is a multimeric glycoprotein present in human plasma and blood vessel subendothelium and plays a central role in the primary hemostasis.[1−3] Each mature subunit is a large single polypeptide chain (2050 amino acids, ~250 kDa) and is covalently linked to its neighboring subunits through disulfide bonds in an N-terminus-to-N-terminus and C-terminus-to-C-terminus fashion.[4−7] VWF is present in the bloodstream as a collection of multimers with a molecular specific weight ranging from 0.5 MDa to more than 20 MDa.[1−3] A mature VWF monomer consists of multiple domains. The domain structure (from N- to C-terminus) is arranged in the following fashion: D′-D3-A1-A2-A3-D4-C1-C2-C3-C4-C5-C6-CK.[5,6,8] Several domains contain one or more binding sites for one of the binding partners of VWF. Notable examples are the A3 domain with the primary binding site for collagen types I and III and the A1 domain with the binding site for glycoprotein Ibα (GPIbα, the primary platelet VWF receptor) and with an additional binding site for collagen VI.[1−3,9] Since the higher order multimers have a larger number of binding sites, their avidity toward platelets is increased, which in turn heightens their propensity to recruit and immobilize platelets and their importance for the hemostasis.[1−3,10]

Under normal physiological conditions, when VWF circulates in flowing blood, VWF adopts a conformation in which the platelet GPIbα binding sites are cryptic (not accessible) because of shielding of the A1 domain by the neighboring domains (A2 and D′D3).[1−3,11−13] VWF can only proceed in adhering platelets (its main function) after exposure of the GPIbα binding sites. This is the case after attachment of VWF to collagen upon, for example, damage to a blood vessel. Another factor regulating of the VWF function is shear stress: the adhesion of platelets through binding of VWF to GPIbα is promoted by high levels of shear stress (blood flows with a wall shear rate of >1000 s^{-1}).[14−16] Shear stress is defined as the

Received: March 5, 2014
Revised: April 19, 2014
Published: April 22, 2014

   dx.doi.org/10.1021/jp5022664 | J. Phys. Chem. B 2014, 118, 5660−5669

component of the stress tensor in the plane of a material cross section, and it can be obtained by multiplying the viscosity of the medium with the local shear rate. The shear rate is the derivative of the fluid velocity in a direction perpendicular to the flow direction.[17−19] This platelet adhesion step forms the basis for further platelet activation, aggregation, and eventually the formation of a platelet plug that seals the damaged vessel wall.[1−3,15] Furthermore, VWF has also been shown to self-associate both under static and flow conditions, and it has been pointed out that this process is also enhanced by shear stress.[2,3,20]

Another known cause that can trigger VWF association to GPIbα in solution besides collagen or certain nonphysiological modulators (botrocetin and ristocetin) is in fact shear stress its self.[1−3,14,21] Shear-stress-induced VWF−GPIbα binding underlies the phenomenon of shear-induced platelet aggregation (SIPA) and entails the formation of the aggregates of platelets under influence of high shear stress (>8 Pa).[14,21,22] The phenomenon of SIPA is presumed to be relevant for the development of malignant thrombosis in occluded and stenosed blood vessels where the shear stresses can exceed 10 Pa.[16]

It is generally believed that shear-stress-induced conformational changes underlie the effects of shear stress on the function of VWF. In 1996, Siedlecki et al.[14] proposed the hypothesis that these conformational changes entail the transition of VWF at high shear stress from a compacted, globular state to a stretched, elongated conformation. In the extended conformation the domains would rearrange in such a way that the shielding of the A1 domains by the A2 or D′D3 domain would be removed.[12,13] Alternatively, recent single molecule force spectroscopy measurements unveiled that A1-GPIbα can adopt a state with a longer lifetime and higher force resistance when subjected to a force exceeding 10 pN.[23] This finding presents a possible alternative or additional mechanism through which the VWF−GPIbα interaction is stabilized and enhanced under high shear stress.

Here we aim to study the influence of shear stress on the conformation of VWF in a glycerol−water Poiseuille flow in order to further uncover the molecular basis of the behavior of VWF in a strong shear flow. Observation of the conformation of VWF is performed with wide-field single molecule fluorescence microscopy[17,19,24−27] in a pressure-driven, flow-rate-controlled Poiseuille flow through a microfluidic device.[28] Wide-field single molecule fluorescence microscopy allows the visualization of individual fluorescently labeled (bio)polymers passing through the focal plane and the subsequent determination of the shape on length scales above the microscope's diffraction-limited lateral spatial resolution (200−250 nm).[17,19,25,26] To overcome the effects of imaging moving objects in flow, an experimental protocol was developed and validated based on stroboscopic excitation, time-gated detection, and the use of buffers with an elevated viscosity.[27] Glycerol is chosen as a cosolvent because it is a small molecule that has many similarities with water (high dipole moment, possibility for hydrogen bonding),[29] its compatibility with biomolecules and proteins in particular (exemplified in its ubiquitous use in protein storage),[29−37] and its previous use in studies on shear-induced protein unfolding.[31] To verify if the sensitivity of the current approach is sufficient for detecting single VWF multimers, the results for labeled VWF are compared with the results of imaging fully extended λ-phage double-stranded DNA labeled with the intercalating fluorophore YOYO-1 in flow.[17,19,26] λ-dsDNA is a good model system for VWF as it also undergoes a transition to an uncoiled, elongated form under influence of shear stress.[17,19,26] In order to examine possible effects of the alteration of the protein's electrostatic charge because of the dense labeling used, experiments were carried out with VWF labeled with a fluorophore having a different charge at neutral pH.[38,39]

EXPERIMENTAL METHODS

Labeling of VWF. Two separate batches of purified plasma VWF (100 μg, Haematologic Technologies Inc.) were fluorescently labeled with ATTO532 (ε(532 nm) = 115 × 10^3 M^{-1} cm^{-1} and ϕ_{fl} = 0.9, ATTO-TEC GmbH)[38] and with ATTO565 (ε(561 nm) = 120 × 10^3 M^{-1} cm^{-1} and ϕ_{fl} = 0.9, ATTO-TEC GmbH)[39] by covalent coupling to the free amine groups of the protein via *N*-hydroxysuccinimidyl chemistry. After labeling, ATTO532 and ATTO565 carry respectively a net charge of −1 and +1 at pH 7.4, which means that the protein charge density will alter when labeling with ATTO532 on free amines.[38,39] Before labeling, the plasma VWF solution was dialyzed three times against PBS (pH 7.4, 10 mM phosphate, Sigma-Aldrich, Inc.) and one time against a carbonate buffer recommended for labeling (pH 8.3, 50 mM $NaHCO_3/Na_2CO_3$, 100 mM NaCl; Sigma-Aldrich, Inc.) at 4 °C under stirring. The labeling reaction was allowed to proceed 1.5 h at room temperature after addition of one of the dyes dissolved in anhydrous DMSO (Acros, Inc.). Purification of the labeled protein from the unreacted dye was achieved via dialysis in PBS with 1 mM Mg^{2+} (two steps, under stirring at 4 °C). Finally, aliquots of the solution were flash frozen in liquid nitrogen and stored at −80 °C.

The VWF antigen concentration and the VWF collagen binding−antigen ratio activity (against collagen type III, Sigma-Aldrich, Inc.) were determined via ELISA assays as described elsewhere.[40] The analysis of the multimer pattern was determined by sodium dodecyl sulfate aragose gel electrophoresis as described elswhere.[40] After separation, VWF was detected using an antihuman VWF-Ig labeled with alkaline phosphatase and an alkaline phosphatase substrate kit (Biorad, Inc.).[40] The relative abundance of each multimer species was calculated by integrating the area under the peak in the density profile of the different lanes in the sample using ImageJ (NIH, Bethesda, MD).[41] To determine to photophysical properties and the degree-of-labeling, the absorption spectra of the VWF−fluorophore conjugates were determined using a PerkinElmer Lambda 40 spectrophotometer. Correction of absorption spectra for the light scattering of the VWF samples was made by fitting a fourth-order polynomical to the regions blue- and red-shifted to the main peak and subtracting the result from the orginal spectrum. The emission spectra were measured using a Spex Fluorolog 3-22 spectrofluorometer (Jobin Yvon-Spec Instruments S. A., Inc.). As references for the fluorescence quantum yield determination, rhodamine 6G (ϕ_{fl} = 0.95) and cresyl violet (ϕ_{fl} = 0.51), both in ethanol, were used.

Fabrication and Calibration of the Microfluidic Flow Cell. Measurements were performed in a Poiseuille flow generated by a syringe pump in a microfluidic flow cell. The shear stress is varied by controlling the shear rate (by setting the flow rate) and the solvent viscosity. The microfluidic flow cell consisted of a glass coverslip (24 × 40 mm^2, grade #1.5; Menzel-Gläser) as bottom part and a poly dimethylsiloxane flow chamber manufactured by soft photolithography (PDMS; Sylgard 184, Dow Corning, Inc.) as top part (see Figure

dx.doi.org/10.1021/jp5022664 | J. Phys. Chem. B 2014, 118, 5660−5669

S2).[28,42] The central part of the channel in the PDMS flow chamber had a rectangular cross section (200 μm width, 70 μm height, 1 cm length) which was connected to the inlet and outlet by two parts (70 μm height, 7 mm length) converging toward the central channel from rectangular channels just below the inlet and outlet (1 mm width, 70 μm height, 4 mm length). Before and after usage the PDMS flow chambers were cleaned by sonication in Milli-Q water. Before usage, the PDMS flow chamber and a thoroughly cleaned coverslip were assembled and placed in a custom metal holder adapted for microscopy and connected to a syringe pump (PHD 2200, Harvard Apparatus) via Teflon tubing.

To calibrate the flow cell, particle image velocimetry experiments with stroboscopic illumination were performed using fluorescent polystyrene beads (0.19 μm diameter excitation 488 nm/emission 520 nm, Bang laboratories) and the wide-field fluorescence microscopy setup described below (configured for excitation with 488 nm light).[28,42,43] The fluid medium was a PBS buffer with 85% (w/w) glycerol (Sigma-Aldrich, Inc.). The determination of a single shear rate consisted of measuring the fluid velocity at different heights (between 0 and 20 μm) in the center of the flow chamber. Figure S2 contains plots of an example of a flow profile measured in center of the channel at 0.36 μL/min and the calibration curve (together with the theoretically calculated curves). When the focal plane is set at a height of 10 μm, the shear stress is essential uniform over the focal volume and can be calculated using the buffer viscocity[28,44] and a calibration equation relating shear rate and applied volumetric flow rate (see Figure S2).

Wide-Field Fluorescence Microscopy. Wide-field imaging was performed on a home-built wide-field fluorescence microscope optimized for single molecule detection, consisting of an inverted microscope (IX71, Olympus) combined with a highly sensitive electron multiplication CCD camera with 512 × 512 pixels (C-9100-13, Hamamatsu).[24,25,27] The excitation light source was, depending on the experiment in question, either a 200 mW 532 nm solid state diode laser (Excelsior, Spectra-Physics), a 100 mW 561 nm solid state diode laser (Sapphire 561 LP, Coherent), or a solid state diode 100 mW 488 nm (Sapphire 488 LP, Coherent). The laser beam was passed through an optical-acoustic modulator (MT80-A3-VIS, AA-Optoelectronics) connected to a digital pulse generator (DG-535, Stanford Research Systems); the latter was, if necessary, also connected to the CCD camera for synchronization. The beam was passed through a combination of an l/2- and 1/4-waveplate to render it circularly polarized. Wide-field illumination was achieved by focusing the expanded laser beam onto the back aperture plane of the microscope objective (60×/1.42 NA oil PlanApo, Olympus).[24,25,27,45] If quasi-TIRF illumination[46] (or HILO mode[45]) was used, the laser beam was aligned through the objective using two mirrors with fine adjustment to control its position and direction.[45,46] Care was taken while doing the alignment to maximize the power after the objective lens. The emission light was collected by the same objective and was passed through an appropriate combination of a dichroic mirror (z532rdc, z561rdc, or z488rdc depending on the excitation wavelength; Chroma) and a long pass filter (HQ545LP, HQ572LP, or HQ505LP depending on the excitation wavelength; Chroma) to fully separate it from the excitation light. Before capturing the image on the CCD camera, it was additionally magnified 2.5× with a projection lens (Olympus). The size of the field of view was in all experiments 54.6 × 54.6 μm^2, or 106.6 × 106.6 nm^2 per pixel.

Observation of Individual DNA Molecules in Solution. For the control experiments studying dsDNA stretching in flow, λ-phage dsDNA (λ-dsDNA) was labeled with the profluorescent, intercalating dye YOYO-1 (ε(488 nm) = 99 × 10^3 M^{-1} cm^{-1} and ϕ_{fl} = 0.38 when bound to dsDNA, $K_{d,dsDNA}$ = 5.46 × 10^5 M^{-1}).[17,19,26,47,48] Depending on the required degree-of-labeling, the appropriate amount of a YOYO-1 stock solution in DMSO (Invitrogen, Inc.) was added to a solution of 5 μg/mL λ-dsDNA in PBS with 1 mM of ethylenediaminetetraacetic acid (EDTA, Sigma) and incubated for 2 h at room temperature, shielded from light.

The microfluidic device, the tubing, and syringes (described above) were blocked by incubation with 0.1% bovine serum albumin (BSA) and 0.01% glucose for over 2 h in order to avoid background fluorescence due to unspecific binding of the eventual unbound fluorophores present in the sample. After the system was perfused with buffer, buffer containing labeled dsDNA was loaded and a flow with a shear rate of 64.0 s^{-1} was started. The buffer was a phosphate based solution (pH 7.4) containing 10 mM KH_2PO_4/Na_2HPO_4 (Sigma), 2 mM NaCl (Sigma), 1 mM EDTA, and 85% (w/w) glycerol. The viscosity of the buffer at room temperature during the experiment (24 °C) was 96.7 mPa·s (measured on a ARES-G2 rheometer with Couette geometry). The final concentration of labeled dsDNA was 8 ng/mL.

Imaging was started only after the system was equilibrated, and the flow in the central channel was stabilized. The wide-field fluorescence microscope (described above) was configured for excitation at 488 nm (optical power after the objective = 29.5 mW) and aligned in quasi-TIRF mode.[46] Both the repetition rate of the light pulses and image capture rate were 28 Hz (limited by the camera read-out speed), and the acquisition time window of the EM-CCD camera was 1 ms. The focal plane was set to a height of 10 μm above the bottom of the channel. Measuring at this height was required because both λ-dsDNA and VWF are driven away from the walls by lift forces present in laminar shear flow.[28,49]

To estimate the length of the imaged DNA molecules, all the molecules passing by in focus were selected by visual inspection.[17,19,26] After selection, an ImageJ plugin (written in Java) determined the average background level around the molecule and calculated the local value for thresholding at half of the object's maximum intensity while traversing the DNA chain. After local thresholding the two points at both extremities of the chain were identified, and the distance between them was calculated (which serves as a good approximation for the chain contour length in these conditions). For DNA chains which were bent in a U-shape, the points at the extremities were identified manually.[19]

The results of the experiments with λ-dsDNA can be found in the Supporting Information. For each of the three labeling conditions tested (19.5, 9.78, and 4.88 YOYO-1 molecules per 100 nm) and excitation with 310 μs pulses, the distribution of estimated contour lengths of imaged λ-dsDNA at a shear stress of 5.5 Pa (shear rate of 39.7 s^{-1}) is composed of a peak situated between 0 and 4 μm and a tail toward higher contour lengths (Figure S3, panels B–D). For the two highest labeling degrees, the distribution extends to contour lengths of ∼16 μm as λ-dsDNA molecules are observed which are fully extended (Figure S3, panel A–C). For the lowest labeling degree no λ-dsDNA chains with an estimated contour length above 10 μm

dx.doi.org/10.1021/jp5022664 | J. Phys. Chem. B 2014, 118, 5660–5669

are observed. Hence, the labeling degree has to be controlled stringently in order to enable the detection of fully extended DNA. The detection of the YOYO-1-labeled λ-dsDNA and in particular the observation of fully extended λ-dsDNA strands can also be achieved with longer excitation pulses (e.g., 360, 420, and 500 μs, data not shown).

Observation of Individually Labeled VWF Molecules in Solution. The entire flow system was first blocked (to avoid unspecific binding of VWF) by incubation with 10 μg/mL unlabeled VWF for 1 h and subsequently with 5 μg/mL VWF, 0.5% BSA, and 0.05% glucose for 1 h. After the system was perfused with a specific buffer and VWF dissolved in the same buffer (concentration between 3.5 and 7 ng/mL dependent on the shear rate used) was loaded, a flow with a shear rate between 12.6 and 64.0 s^{-1} was applied (given shear stresses of 0.44−12.4 Pa). For each sampled shear stress level, two separate measurements were made. The specific buffers used for imaging were PBS buffers (pH 7.4; 10 mM KH_2PO_4/Na_2HPO_4, 137 mM NaCl, 2 mM KCl, and 1 $MgCl_2$) with 70, 85 or 88.5% (w/w) glycerol, respectively. The viscosity of these buffers at the room temperature during the experiments (22 ± 0.5 °C) was 23.4, 162.4, and 193.8 mPa·s, respectively. The viscosity of these buffers was determined as described above.

Imaging was started only after the flow has stabilized and attained the expected velocity profile. The wide-field fluorescence microscope (described above) was configured for excitation at either 532 nm (optical power after the objective = 67−70 mW) or 561 nm (44−47 mW) and was aligned in quasi-TIRF mode[46] (also known as HILO mode[45]). The focal plane was set to a height of 10 μm above the bottom of the center of the central channel, at a distance of approximately 5 mm from the entrance of the central channel. The lower bounds for the time it takes a VWF multimer to enter the central channel of the microfluidic and pass through the focal plane varied from 33.3 s (at 12.6 s^{-1}) and 6.9 s (at 64.0 s^{-1}). The pulse lengths were varied from 1.2 ms (at 12.6 s^{-1}) to 310 μs (at 64.0 s^{-1}) depending on the applied shear rate and set just under or at the time it would take a particle moving in the focal plane to traverse a distance equal to the lateral resolution of the microscope (or diffraction limit). The diffraction limit is defined by the Raleigh criterion (D_{limit} = 0.61 × (λ/(NA)), where λ is the wavelength of the emission light and NA is the numerical aperture of the objective) and was calculated to be 228 nm in the case of VWF-ATTO532 and 251 nm of VWF-ATTO565. The flow velocity at 10 μm height was calculated according to the equation for a Poiseuille flow in a rectangular channel. Both the repetition rate of the light pulses and image capture rate were 28 Hz, and the acquisition time window of the EM-CCD camera was either 1, 1.2, or 1.5 ms depending on the laser pulse length. A schematic overview of the parameters used for all shear stress levels measured is provided in the Supporting Information (Table S2, for the experiments with VWF-ATTO532, and Table S3, for the experiments with VWF-ATTO565).

Analysis of the Observed Individual Labeled VWF Molecules. The dimensions of the observed VWF molecules were extracted by fitting the profiles along the direction of the major and minor axis of the molecules running through the centroid with a linear combination of diffraction-limited Gaussians or a single Gaussian model, respectively. The observed molecules were first selected by visual inspection[17,19,26] and later on given as input in a custom written Java program (based on ImageJ's advanced programming interface and Matlab's nonlinear least-squares curve fitting routine).

To take in account the possible rotation of the elongated molecules perpendicular to the axis of the flow, the selected objects were first fitted with an asymmetric two-dimensional Gaussian, which was allowed to rotate around its central axis. Most molecules have however their major axis aligned with (and their minor axis perpendicular to) the direction of the flow. For molecules with a fitted ellipticity below 1.35, the flow direction was taken automatically as the major axis because of the sensitivity of the axis determination to noise in this case. The same was done for molecules with a rotation angle below 10°.

The end points of the major axis profiles were determined by starting from both ends of the profiles and finding the first point at both ends for which (1) the intensity was higher than the average of the average background and the molecule's maximum intensity and (2) the intensity difference with the preceding point was higher than the difference with the following point. For both of the end points and for every pixel in between the end points a diffraction-limited Gaussian with its center placed on the corresponding pixel was added to the fit function. The standard deviation of the diffraction-limited Gaussians was taken to be 81.4 nm for the analysis of VWF-ATTO532 and 87.3 nm for the analysis of VWF-ATTO565 (values determined by fitting a simulated PSF). The begin amplitudes were computed by linear least-squares fitting with the constraint that they should be positive. The positions of the intermediate Gaussians were set invariant during fitting while the position of the Gaussian at both ends was allowed to vary within ±1.2 pixel units. After fitting the results were visually inspected and changes were made to the location of the end points with subsequent refitting if necessary.

EXPERIMENTAL RESULTS

Shear Stress Dependence of the Extension of VWF-ATTO532 in Shear Flow. Figure 1 displays the recorded image for three VWF-ATTO532 molecules passing through the focal volume detected at a local shear stress 10.4 Pa and in solution in a PBS buffer with 85% (w/w) glycerol (additional examples are given in Figure S4). The collagen binding properties and multimer pattern are preserved after labeling (see Table S1 and Figure S1). The categories of shapes represented by these three examples encompass nearly all observed multimers in each measurement. The molecule on the top of Figure 1 (panel A) is an example of a small, isotropic shaped VWF molecule, which resembles somewhat the point spread function of the microscope. On the other hand, panels in the middle and at the bottom of Figure 1 contain images of VWF multimers which have an anisotropic shape and are extended along one axis to a smaller or larger degree. This example shows that at 10.4 Pa, which in the high end of the current range of sampled shear stresses, certain VWF-ATTO532 multimers adopt an extended conformation. However, if an influence of the shear stress on the conformation of VWF-ATTO532 is to be established, a comparison needs to be made between the occurrence of multimers with an elongated conformation at different shear stresses.

In order to reveal detailed information on shear stress dependency of the occurrence of the different types of observed multimer conformations, the shapes of the multimers are characterized by fitting the profiles along the major and minor

dx.doi.org/10.1021/jp5022664 | J. Phys. Chem. B 2014, 118, 5660−5669

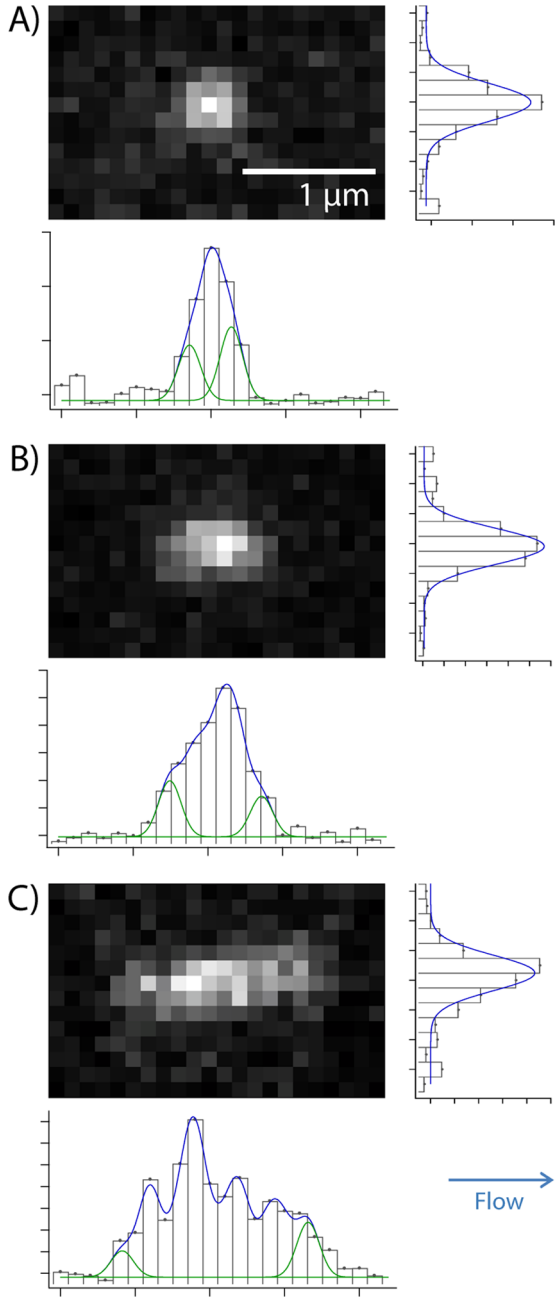

Figure 1. Three examples of VWF-ATTO532 multimers observed with wide-field single molecule fluorescence microscopy in a shear flow of 10.4 Pa. The wide-field images of three molecules passing through the focal volume set at 10 μm height have been obtained by using stroboscopic excitation (310 μs pulses; in a quasi-TIRF configuration) in order to reduce the movement of the molecules during image aquisition. The image intensity profiles along the major axis and minor axis of the molecules are plotted respectively beneath and left of the images (in gray). The horizontal axis of the major axis profile graph denotes pixel position and the vertical axis recorded intensity (in au). For the minor axis profile graph the axis are reversed. Both plots contain also the fitted models (in blue) and, in the case of the major axis plot, the diffraction-limited Gaussians at both ends (in green). The dimensions, given as (center-to-center distance; fitted Gaussian width), respectively, are (A) (0.301 μm, 0.137 μm), (B) (0.554 μm, 0.129 μm), and (C) (1.34 μm, 0.129 μm). Imaging was performed in PBS with 85% (w/w) glycerol.

axis (both perpendicular to one another) for 2000−2600 molecules with respectively a linear combination of diffraction-limited Gaussians or a single Gaussian (see Experimental Methods for details). For the major axis profile the center-to-center distance is computed, which is the distance between the centers of the Gaussian at both ends of the fitted function (results shown in Figure 2). For the minor axis the width of the Gaussian is considered (results shown in Figure 3 and Figure S5). For the three examples shown in Figure 1 the two profiles together with the results of fitting both profiles are plotted alongside the raw image.

The changes in shapes as a function of shear stress are seen in the distributions of the center-to-center distances of the major axis profiles rather than in the distributions of the standard deviations of the Gaussian fit functions of the minor axis profiles (Figures 2 and 3 and Figure S5). This is apparent from a comparison of the histograms and the graphs plotting the means and standard deviations (given in Figures 2E and 3B, respectively). Each obtained minor axis width distribution is Gaussian shaped with a center near 0.130−0.140 μm (Figure 3B and Figure S5) and a standard deviation in the range of 0.022−0.031 μm (Figure 3 and Figure S4). They do not display any further dependency on shear stress, in contrast the center-to-center distance distributions.

Comparison of the histograms of the center-to-center distance for VWF-ATTO532 at the different sampled shear stresses indicates that, starting from 2.05 Pa, a limited fraction of VWF multimers are extended with major axis dimensions well above the population mean (Figure 2). Moreover, the size of this subfraction increases as a function of shear stress (Figure 2F). The distributions of the center-to-center distance have two main features: a peak and a tail. The peak centered around 0.350−0.400 μm contains the grand majority of the observed molecules (64−87% fall in a bin between 0.200 and 0.500 μm) and is present for every measurement, regardless of the shear stress (0.44−12.4 Pa) or glycerol content of the buffer (being either 70, 85, or 88.5% (w/w)). The tail spans the range of high center-to-center distances from ∼0.700 to ∼2.000 μm, has a magnitude strongly dependent on shear stress, and contains only a small fraction of the observed molecules (<14%). This observation corresponds with the types of shapes seen by eye mentioned earlier (Figure 1) and is illustrated by the histograms of measurements at 0.44, 2.48, 6.44, and 10.4 Pa shown in panels A through D of Figure 2. Almost no multimers with a center-to-center distance above 0.700 μm are observed at the lowest three sampled shear stress levels (see Figure 2A,F), while this fraction (which is a metric for the relative magnitude of the tail) increases nearly linearly in magnitude with increasing shear stress from 2.05 to 12.4 Pa. The standard deviation and, to a small extent, also the mean of the VWF center-to-center distributions similarly show a rising trend as a function of shear stress (Figure 2E), which is expected when the tail of a distribution gains in weight. However, the relative number of VWF multimers within the observed population is, even at high shear stresses, comparatively small as it does never exceed 14%. The increase of the fraction of VWF-ATTO532 molecules with an center-to-center distance above 0.7 μm above ∼2.0 Pa signifies that VWF-ATTO532 can indeed exhibit conformational changes in the form of an extension in shear flow. This is supported by the images of the multimers displayed in Figure S4. At relatively moderate shear stresses, there are rare occasions in which a multimer traverses the focal

dx.doi.org/10.1021/jp5022664 | J. Phys. Chem. B 2014, 118, 5660−5669

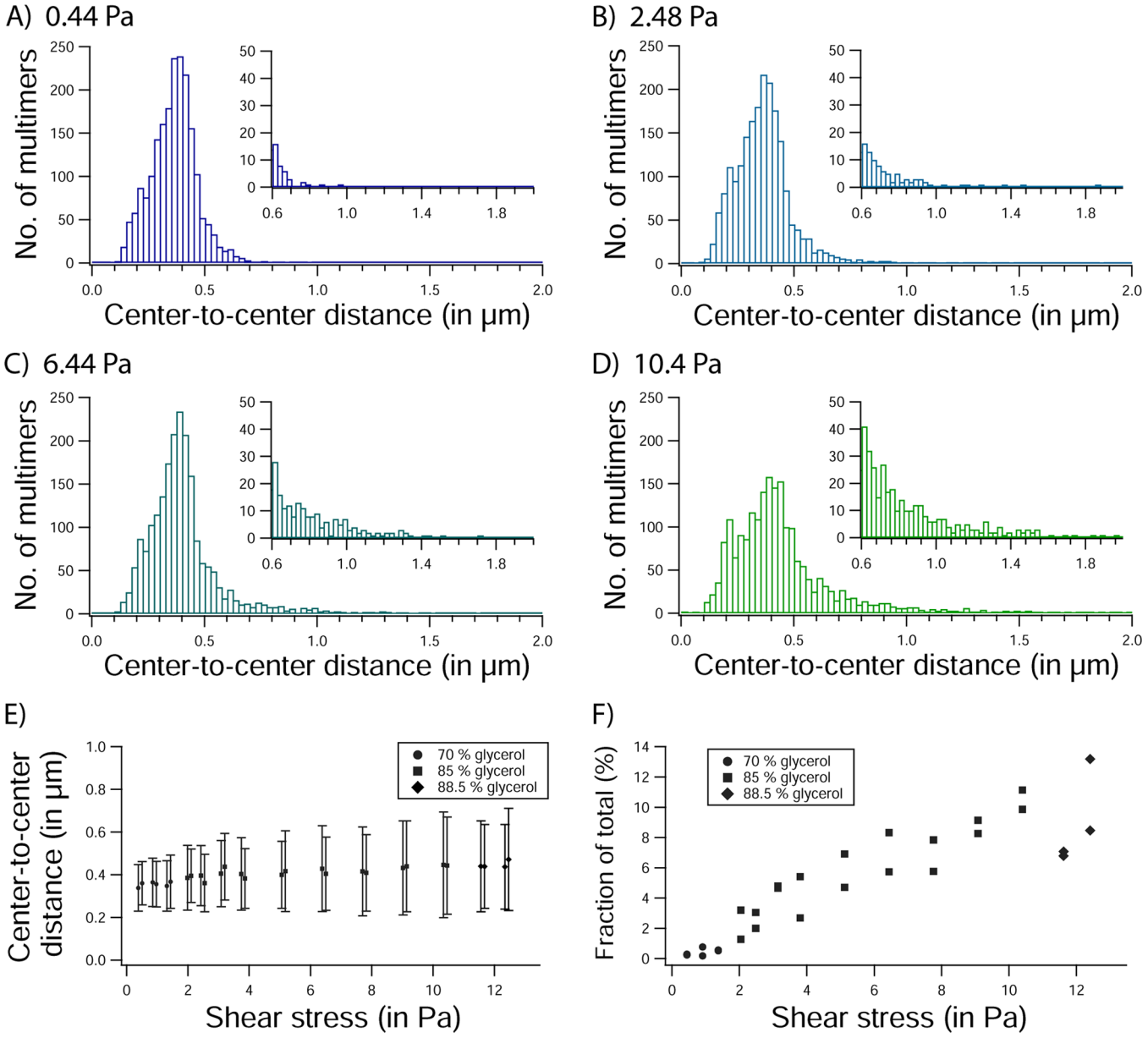

Figure 2. Analysis of the profiles along the major axis for VWF-ATTO532. Each profile has been fitted with a linear combination of diffraction-limited Gaussians (see Experimental Methods). (A–D) Distribution of the distances between the diffraction-limited Gaussians fitted at both ends of the profile (the center-to-center distance) for (A) 0.44 (measurement in 70% (w/w) glycerol), (B) 2.48, (C) 6.44, and (D) 10.4 Pa (measurement in 85% (w/w) glycerol). For each histogram at least 2000 molecules have been analyzed. (E) Average center-to-center distance plotted in function of shear stress. The error bars denote the standard deviation. (F) Fraction of multimers with a center-to-center distance above 0.7 μm. Inset in each histogram contains a zoom-in on the tail of each distribution.

plane while exhibiting visible conformational changes (both extension and recoiling of the chain).

Independence of the Extension of VWF of Label Charge. The observations for VWF-ATTO565 shown almost no significant differences with respect to the observations for VWF-ATTO532 (data shown in Supporting Information Figures S6–S8). This signifies that the extension of VWF in shear flow is not influence by the changes in protein charge and pI after labeling with rhodamine derivative.[38,39]

DISCUSSION

Detection of Individual VWF Multimers in Flow. In order to overcome the artifacts imposed on imaging by the movement of VWF across the focal volume (being artificial object elongation) during image acquisition, stroboscopic illumination was used here.[24,25,27] However, the use of short excitation times poses limitations on the obtainable detection sensitivity, which in turn sets limits on the fluid velocities at which we still can attain a sufficient detection sensitivity.[24,25] Because the excitation/integration periods employed here are below those typically used for wide-field single molecule fluorescence microscopy,[17,19,24–27] a control is needed to ascertain if it is possible to image uncoiled VWF multimers with a sufficient signal-to-noise ratio and, if so, what labeling density is required.

As a control, λ-dsDNA-YOYO-1 was visualized in flow on the same setup used for VWF detection (results displayed in Figure S3).[17,19,26,47,48] λ -dsDNA is a good model system for

dx.doi.org/10.1021/jp5022664 | J. Phys. Chem. B 2014, 118, 5660–5669

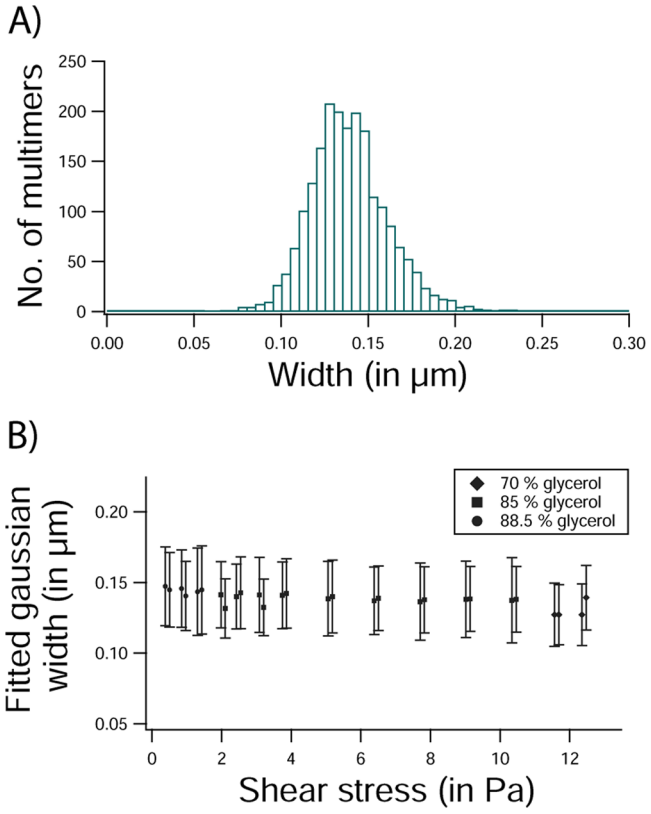

Figure 3. Analysis of the profiles along the minor axis to the flow for VWF-ATTO532. (A) Distribution of the width of the fitted Gaussian model for a shear stress of 6.44 Pa (buffer contained 85% (w/w) glycerol). (B) Average width plotted in function of shear stress. The error bars denote the standard deviation of the width distribution.

VWF as the nucleotide chain can adopt an extended linear form in a shear flow with a sufficiently high shear rate.[17,19,26] This has been well studied both experimentally and by simulations.[17−19,26,50,51] A fully extended λ-dsDNA chain (end-to-end length = 16 μm) represents a one-dimensional object with a (near) homogeneous mass distribution, and thus a linear labeling density can be inferred.[19,27] The observation of both VWF-ATTO532 and VWF-ATTO565 allows us to treat VWF in flow as a one-dimensional object with excellent approximation. Every measured distribution of minor axis width has a mean in the vicinity of 0.130−0.140 μm, which is slightly larger than expected for fitting a simulated point spread function (81.4 nm for imaging at 532 and 87.3 nm at 561 nm). Taking into account the slight defocusing of the molecules passing at the top and the bottom of the focal volume (which extends several hundred nanometers along the axial direction) and the noise on the image, the actual width of the VWF multimers along this axis is in fact smaller than the diffraction limit.[17,19,24−27] This would be in agreement with all previously published studies on the structure of VWF.[4−6,14,52,53]

As the background photon counts and detector dark counts in both the λ-dsDNA and the VWF experiments are very similar, the signal-to-noise ratio is mainly determined by the fluorophore fluorescence photon counts.[24] The differences between the experiments with DNA-YOYO-1 and VWF-ATTO532/ATTO565 are related to four factors (fluorophore extinction coefficient and fluorescence quantum yield, excitation power and filter, and dichroic transmission efficiency, values summarized in Table S4). Because the collected fluorescence photon count has a linear dependence on all four factors, they would lead to a difference of a factor 5.14/4.21 between fluorescence photon count in imaging an equally dense YOYO-1 or ATTO532/ATTO565 labeled object with the respective current microscopy setup configurations.[24,25] As is apparent from Figure S3A, individual fully extended λ-dsDNA chains labeled with 9.78 YOYO-1 fluorophores per 100 nm are observed using the shortest laser pulse width used for VWF-ATTO532/ATTO565 detection (310 μs) with the current experimental approach. The same fluorescence signal and signal-to-noise ratio should be obtained (at least in principle) when imaging fully elongated VWF multimers labeled with 1.90 ATTO532 fluorophores per 100 nm or 2.32 ATTO565 fluorophores per 100 nm under the present conditions. This requirement will be met with the labeled VWF used for this study if the length of a single monomer would be less than 100 nm for VWF-ATTO532 or less than 82 nm for VWF-ATTO565. The results presented in Figure S3 and discussed here are obtained with an illumination time of 310 μs because this is the shortest pulse length used for imaging VWF-ATTO532/ATTO565. While also having measured with longer excitation pulses, the signal-to-noise ratio is expected to be the lowest in the former case as the number of collected fluorescence photons is proportional to the excitation pulse duration.[24,25,27] Longer pulse widths were also tested, and detection of fully extended λ-dsDNA was routinely possible.

The literature on the structure of VWF strongly indicates that VWF will not extend to such a degree that the used labeling density would result in problems for single molecule detection. Several papers strongly suggest a value around 60−70 nm for the length of a VWF monomer in an elongated multimer.[4−6,14,52,53] The largest multimers of which we can verify the presence in our sample by multimer gel analysis are composed of 22 monomers, which when extended would have an end-to-end length when elongated of 1540 nm. Given that (1) we only rarely observe VWF molecules with a center-to-center distance above 1.0 μm, that (2) VWF multimers with a length above 1.5 μm are hardly ever seen, and that (3) we observe the tail of the center-to-center distributions gradually increasing in weight in function of shear stress, it seems that VWF does not elongate to such an extent that the monomers adopt lengths exceeding what has been previously reported. Finally, if this were not the case and the density requirements for single molecule detection were not fulfilled, molecules with progressively increasing center-to-center distance above 2.0 μm but with (very) low, decreasing signal-to-noise ratios should be observed, something which is not the case here.

Extension of VWF under Shear Stress. The current results allows us to conclude that at least a small fraction of VWF multimers does experience a extension of their multimer chains. A combination of four factors can constitute an explanation why only a small fraction of extended VWF multimers are observed: (1) The limits on the lateral spatial resolution of optical microscopy[17,19,24−27] prevent the detection of extension of only limited part of the multimer chain of VWF or of conformational alterations on a domain or subdomain level.[12,13,23,52,53] (2) The VWF used here contains a considerable fraction of smaller multimers of which the elongated form may not have a total length exceeding the diffraction limit (dimers and tetramers constitute together about 18−30% of each sample; see Figure S1).[4−6,14,52] (3) The time between the onset of maximum shear stress in the central channel of our microfluidic flowcell and passage through the

dx.doi.org/10.1021/jp5022664 | J. Phys. Chem. B 2014, 118, 5660−5669

detection volume may be insufficient for the system to reach equilibrium. (4) VWF may exhibit a constant extending and recoiling behavior in a regime where the forces on the multimer chain can overcome the interdomain interactions. In this case, only a part of the population of VWF multimers will have at any given time a fully or nearly fully extended conformation. Ideal polymer chains (which lack specific intra- and intermolecular associative interactions) such as DNA display in shear flow a constant competition between chain extension and chain (re)collapse.[17,19,26] This behavior is due to the two components of a shear flow: the elongational component causing stretching of the DNA while the rotational component causes end-over-end tumbling and thus collapsing. The fact that we can (although very rarely) observed VWF multimers traversing the focal volume while switching from a compacted, isotropic shape to an extended shape and *vice versa* provides some support for this hypothesis (Figure S4). These factors leave open the possibility that the VWF currently observed in a compacted state may also have undergone (partial) elongation or might undergo elongation at a later time.

A reasonable explanation for the apparent shear stress threshold near 2−2.5 Pa for extension of VWF involves the specific noncovalent interdomain interactions, such as between the A1 domain and the D′D3 and the A2 domain, respectively, which also play a role in the self-association of VWF.[11−13] These interactions stabilize the compacted state of VWF and oppose flow-induced deformations and would thus need to be overcome by a sufficiently strong force before any extension of the VWF chain can occur. Moreover, the different interdomain interactions[11] may each possess a different strength (dissociation constant) which are then progressively broken as the shear stress grows, providing a possible explanation for the incremental growth the percentage of extended VWF multimers. However, the existence of a shear stress threshold would also constitute an important deviation from the behavior of ideal polymers in shear flow. In polymer physics, the configuration of an ideal polymer chain in shear flow is determined by the amount of local shear rate, and not shear stress, relative to the relaxation time of the Rouse-like relaxation modes of the polymer.[17,19,51] In the present case, one can suspect that the reverse is true: shear stress rather than shear rate governs VWF extension because VWF differs from an ideal polymer chain (well approximated by e.g. λ-dsDNA) because of the presence of specific interdomain interactions. However, the current experiments do not allow us to distinguish whether VWF extension in shear flow is ultimately dependent on shear stress or shear rate. One could propose an argument based on the observed differences between the measurements performed with the buffers with 70 and 85% (v/v) glycerol. These are done in a similar range of shear rates but in different shear stress ranges. However, this is a naive reasoning as the near 6-fold difference in viscosity is bound to give rise to different relaxation times for VWF.[17,19,51] An indirect indication that shear stress rather than shear rate controls the deformation of VWF in shear flow is provided by the observation that SIPA is strictly dependent on the former.[21]

The dimensions of the extended VWF multimers observed here lie in the range set out in previous studies of the structure of VWF[4−6] and on VWF stretching in shear flow (by Siedlecki et al.)[14] The apparent threshold for VWF shear flow-induced extension found here is also consistent with the observations of Siedlecki et al.[14] Ensemble averaging[24,25] may explain the differences with the report of Singh et al.,[52,53] who have done neutron scattering experiments on VWF in buffer.

In contrast to the results reported here, Schneider et al.[55] describe a sharp, well-defined conformational transition around a critical shear rate of 5000 s^{-1} in PBS and elongation of VWF multimers above this point to end-to-end length up to 10 μm. Their technique to overcome the artifacts linked to imaging objects in flow relied on postacquisition image correction based on simultaneous measurement of the fluid velocity with fluorescent beads. The difficulty with this method lies in the fact that extremely high axial localization precisions, and therefore image signal-to-noise ratios need to be obtained in order to get a sufficiently low error in particle velocity estimation.[24,25,27] We have tried to repeat these experiments with our measurement setup by trying to measure in PBS at shear rates of 1000−10000 s^{-1}. We could not achieve single molecule imaging with such short excitation periods neither for VWF-ATTO532 nor for λ-dsDNA-YOYO-1 because of the too small excitation pulse widths (2−20 μs), despite of all of the optimizations made.[24,25] Because imaging VWF on a single molecule level in flow at the required shear stresses was not possible in regular water-based buffers, glycerol−water buffers are used here in order to obtain the necessary shear stress with reduced shear rates/fluid velocities.[14,21,28]

The results of the present study are believed to be relevant for VWF extension in more physiological relevant conditions (regular buffers, plasma, or blood) given that proteins have essentially the same conformation in water or in glycerol.[29,30,32−34] Many studies can be found in the literature which point out that proteins exhibit a small compaction of their structure in water−glycerol but otherwise retain their secondary and tertiary structure.[30−37] Several studies demonstrate that enzymes retain their activity in mixtures of water−glycerol with glycerol levels up to 90% (w/w).[32,34] Dissociation constants for protein−protein interactions in water−glycerol have been found to lie within 1 order of magnitude compared to their counterparts in aqueous buffers.[34−36] Proteins do have an elevated stability toward denaturation in water−glycerol (assumed to be due to shielding of the hydrophobic interior).[29−31] This suggests that VWF extension will occur at lower shear stresses (if some level of shear stress rather than shear rate is required) in physiological conditions than observed here if (partial) denaturation of (parts of) the polypeptide chain should be involved in the process of extension.

CONCLUSIONS

We demonstrate the feasibility of detecting individual VWF multimers in a Poiseuille flow at shear rates up to 64.0 s^{-1} with single molecule wide-field fluorescence microscopy. At shear stresses above an apparent threshold of around 2.0−2.5 Pa, in water−glycerol buffers VWF can attain a conformation which is extended along one molecular axis with lengths up to 2.0 μm. The probability for a multimer to make such a transition increases as a function of shear stress.

The current findings support the hypothesis on the existence of a large-scale conformational transition for VWF in shear flow, as proposed by Siedlecki et al.[14] to explain the activation of VWF under high shear stress in buffer or plasma. The current study does not rule out any conformational transitions on subdiffraction limit length scales that have also been described in the literature. Verification of whether shear stress or shear rate ultimately determines the conformational

dx.doi.org/10.1021/jp5022664 | J. Phys. Chem. B 2014, 118, 5660−5669

dynamics of VWF in shear flow would reveal information about the factors governing the dynamics of VWF extension in shear flow (e.g., influence of interdomain interactions vs dynamics of the Rouse-like relaxation modes).

■ ASSOCIATED CONTENT

Supporting Information

Table S1: overview of the functional and photophysical properties of VWF-ATTO532 and VWF-ATTO565 after labeling; Table S2: overview of the measurement parameters used for VWF-ATTO532; Table S3: overview of the measurement parameters used for VWF-ATTO565; Table S4: comparison of the photophysical and imaging parameters for imaging YOYO-1 stained dsDNA and VWF-ATTO532/ATTO565; Figure S1: multimer gel analyze of VWF labeled with ATTO532 and ATTO565; Figure S1: multimer gel analyze of VWF labeled with ATTO532 and ATTO565; Figure S2: overview and calibration of the microfluidic flow cell; Figure S3: imaging the extension of individual λ-DNA strands in a shear flow; Figure S4: examples of VWF multimers which change their conformation while passing through the focal plane; Figure S5: distribution of the width of the profiles along the perpendicular axis for VWF-ATTO532; Figure S6: three examples of VWF-ATTO565 multimers observed in a shear flow of 12.4 Pa; Figure S7: analysis of the profiles along the major axis to the flow for VWF-ATTO565; Figure S8: analysis of the width of the Gaussian fit of the profiles along the minor axis for VWF-ATTO565. This material is available free of charge via the Internet at http://pubs.acs.org.

■ AUTHOR INFORMATION

Corresponding Author

*E-mail johan.hofkens@chem.kuleuven.be (J.H.).

Present Address

K.D.C.: Beth Israel Deaconess Medical Center, 330 Brookline Avenue, Boston, MA 02215.

Notes

The authors declare no competing financial interest.

■ ACKNOWLEDGMENTS

We thank Tom Verwijlen for helping with the rheological measurements. R.V. acknowledges the support of the Institute for the Promotion of Innovation through Science and Technology in Flanders (IWT-Vlaanderen) of the Flemish Government through a PhD scholarship. The research leading to these results has received funding from the European Research Council under the European Union's Seventh Framework Programme (FP7/2007-2013)/ERC Grant Agreement No. 291593 FLUOROCODE), from the Flemish government in the form of long-term structural funding "Methusalem" grant METH/08/04 CASAS, from the "Fonds voor Wetenschapplijk Onderzoek Vlaanderen" (FWO grants G0607.09, G0554.10, G0413.10, G0697.11, and G0197.11), and from the Hercules Foundation (HER/08/021).

■ ABBREVIATIONS

bp, base pair; BSA, bovine serum albumin; CCD, charge coupled device; DOL, degree of labeling; dsDNA, double-stranded DNA; EDTA, ethylenediaminetetraacetic acid; GP Ibα, glycoprotein Ibα; HILO, highly inclined illumination; PDMS, polydimethyldisiloxane; SIPA, shear-enhanced platelet aggregation; quasi-TIRF, quasi-total internal reflection; VWF, von Willebrand factor; VWF:Ag, VWF antigen level; VWF:CB, VWF collagen binding.

■ REFERENCES

(1) Sadler, J. E. Biochemistry and Genetics of von Willebrand Factor. *Annu. Rev. Biochem.* **1998**, *67*, 395−424.

(2) De Meyer, S. F.; Deckmyn, H.; Vanhoorelbeke, K. Von Willebrand Factor to the Rescue. *Blood* **2009**, *113*, 5049−57.

(3) Lenting, P. J.; Casari, C.; Christophe, O. D.; Denis, C. V. Von Willebrand Factor: The Old, the New and the Unknown. *J. Thromb. Haemost.* **2012**, *10*, 2428−37.

(4) Slayters, H.; Loscalzoyl, J.; Bockenstedt, P.; Handin, R. I. Native Conformation of Human von Willebrand Protein a. *J. Biol. Chem.* **1985**, *260*, 8559−8563.

(5) Fretto, L.; Fowler, W. E.; McCaslin, D. R.; Erickson, H. P.; Mckee, P. A. Substructure of Human von Willerand Factor. *J. Biol. Chem.* **1986**, *261*, 15679−15689.

(6) Shelton-Inloes, B. B.; Titanis, K.; Sadler, J. E. cDNA Sequences for Human von Willebrand Factor Reveal Five Types of Repeated Domains and Five Possible Protein Sequence Polymorphisms. *Biochemistry* **1986**, *25*, 3164−3171.

(7) Huang, R.-H.; Wang, Y.; Roth, R.; Yu, X.; Purvis, A. R.; Heuser, J. E.; Egelman, E. H.; Sadler, J. E. Assembly of Weibel-Palade Body-like Tubules from N-Terminal Domains of von Willebrand Factor. *Proc. Natl. Acad. Sci. U. S. A.* **2008**, *105*, 482−7.

(8) Zhou, Y.-F.; Eng, E. T.; Zhu, J.; Lu, C.; Walz, T.; Springer, T. A. Sequence and Structure Relationships within von Willebrand Factor. *Blood* **2012**, *120*, 449−58.

(9) De Ceunynck, K.; De Meyer, S. F.; Vanhoorelbeke, K. Unwinding the von Willebrand Factor Strings Puzzle. *Blood* **2013**, *121*, 270−7.

(10) De Ceunynck, K.; Rocha, S.; Feys, H. B.; De Meyer, S. F.; Uji-i, H.; Deckmyn, H.; Hofkens, J.; Vanhoorelbeke, K. Local Elongation of Endothelial Cell-Anchored von Willebrand Factor Strings Precedes ADAMTS13 Protein-Mediated Proteolysis. *J. Biol. Chem.* **2011**, *286*, 36361−7.

(11) Ulrichts, H.; Vanhoorelbeke, K.; Girma, J. P.; Lenting, P. J.; Vauterin, S.; Deckmyn, H. The von Willebrand Factor Self-Association Is Modulated by a Multiple Domain Interaction. *J. Thromb. Haemost.* **2005**, *3*, 552−61.

(12) Ulrichts, H.; Udvardy, M.; Lenting, P. J.; Pareyn, I.; Vandeputte, N.; Vanhoorelbeke, K.; Deckmyn, H. Shielding of the A1 Domain by the D′D3 Domains of von Willebrand Factor Modulates Its Interaction with Platelet Glycoprotein Ib-IX-V. *J. Biol. Chem.* **2006**, *281*, 4699−707.

(13) Martin, C.; Morales, L. D.; Cruz, M. a. Purified A2 Domain of von Willebrand Factor Binds to the Active Conformation of von Willebrand Factor and Blocks the Interaction with Platelet Glycoprotein Ibalpha. *J. Thromb. Haemost.* **2007**, *5*, 1363−70.

(14) Siedlecki, C. a; Lestini, B. J.; Kottke-Marchant, K. K.; Eppell, S. J.; Wilson, D. L.; Marchant, R. E. Shear-Dependent Changes in the Three-Dimensional Structure of Human von Willebrand Factor. *Blood* **1996**, *88*, 2939−50.

(15) Savage, B.; Saldívar, E.; Ruggeri, Z. M. Initiation of Platelet Adhesion by Arrest onto Fibrinogen or Translocation on von Willebrand Factor. *Cell* **1996**, *84*, 289−97.

(16) Westein, E.; van der Meer, A. D.; Kuijpers, M. J. E.; Frimat, J.-P.; van den Berg, A.; Heemskerk, J. W. M. Atherosclerotic Geometries Exacerbate Pathological Thrombus Formation Poststenosis in a von Willebrand Factor-Dependent Manner. *Proc. Natl. Acad. Sci. U. S. A.* **2013**, *110*, 1357−62.

(17) Smith, D. E.; Babcock, H. P.; Chu, S. Single-Polymer Dynamics in Steady Shear Flow. *Science* **1999**, *283*, 1724−1727.

(18) Lee, J.; Shaqfeh, E.; Muller, S. Dynamics of DNA Tumbling in Shear to Rotational Mixed Flows: Pathways and Periods. *Phys. Rev. E* **2007**, *75*, 040802.

(19) Leduc, P.; Haber, C.; Bao, G.; Wirtz, D. Dynamics of Individual Flexible Polymers in a Shear Flow. *Nature* **1999**, *399*, 564−566.

(20) Savage, B.; Sixma, J. J.; Ruggeri, Z. M. Functional Self-Association of von Willebrand Factor during Platelet Adhesion under Flow. *Proc. Natl. Acad. Sci. U. S. A.* **2002**, *99*, 425−30.
(21) Shankaran, H.; Alexandridis, P.; Neelamegham, S. Aspects of Hydrodynamic Shear Regulating Shear-Induced Platelet Activation and Self-Association of von Willebrand Factor in Suspension. *Blood* **2003**, *101*, 2637−2645.
(22) Depraetere, H.; Ajzenberg, N.; Girma, J. P.; Lacombe, C.; Meyer, D.; Deckmyn, H. Baruch, D. Platelet Aggregation Induced by a Monoclonal Antibody to the A1 Domain of von Willebrand Factor. *Blood* **1998**, *91*, 3792−9.
(23) Kim, J.; Zhang, C.-Z.; Zhang, X.; Springer, T. A. A Mechanically Stabilized Receptor-Ligand Flex-Bond Important in the Vasculature. *Nature* **2010**, *466*, 992−5.
(24) Moerner, W. E.; Fromm, D. P. Methods of Single-Molecule Fluorescence Spectroscopy and Microscopy. *Rev. Sci. Instrum.* **2003**, *74*, 3597.
(25) Wöll, D.; Braeken, E.; Deres, A.; De Schryver, F. C.; Uji-i, H.; Hofkens, J. Polymers and Single Molecule Fluorescence Spectroscopy, What Can We Learn? *Chem. Soc. Rev.* **2009**, *38*, 313−28.
(26) Quake, S. R.; Babcock, H.; Chu, S. The Dynamics of Partially Extended Single Molecules of DNA. *Nature* **1997**, *388*, 151−4.
(27) Flors, C.; Hotta, J.; Uji-i, H.; Dedecker, P.; Ando, R.; Mizuno, H.; Miyawaki, A.; Hofkens, J. A Stroboscopic Approach for Fast Photoactivation-Localization Microscopy with Dronpa Mutants. *J. Am. Chem. Soc.* **2007**, *129*, 13970−7.
(28) Stone, H. A.; Stroock, A. D.; Ajdari, A. Engineering Flows in Small Devices. *Annu. Rev. Fluid Mech.* **2004**, *36*, 381−411.
(29) Timasheff, S. N. The Control of Protein Stability and Association by Weak Interactions with Water: How Do Solvents Affect These Processes? *Annu. Rev. Biophys. Biomol. Struct.* **1993**, *22*, 67−97.
(30) Knubovets, T.; Osterhout, J. J.; Connolly, P. J.; Klibanov, A. M. Structure, Thermostability, and Conformational Flexibility of Hen Egg-White Lysozyme Dissolved in Glycerol. *Proc. Natl. Acad. Sci. U. S. A.* **1999**, *96*, 1262−7.
(31) Ashton, L.; Dusting, J.; Imomoh, E.; Balabani, S.; Blanch, E. W. Shear-Induced Unfolding of Lysozyme Monitored in Situ. *Biophys. J.* **2009**, *96*, 4231−6.
(32) Zancan, P.; Sola-Penna, M. Trehalose and Glycerol Stabilize and Renature Yeast Inorganic Pyrophosphatase Inactivated by Very High Temperatures. *Arch. Biochem. Biophys.* **2005**, *444*, 52−60.
(33) Garcia-Manyes, S.; Dougan, L.; Fernández, J. M. Osmolyte-Induced Separation of the Mechanical Folding Phases of Ubiquitin. *Proc. Natl. Acad. Sci. U. S. A.* **2009**, *106*, 10540−5.
(34) Zhou, Y.-L.; Liao, J.-M.; Chen, J.; Liang, Y. Macromolecular Crowding Enhances the Binding of Superoxide Dismutase to Xanthine Oxidase: Implications for Protein-Protein Interactions in Intracellular Environments. *Int. J. Biochem. Cell Biol.* **2006**, *38*, 1986−94.
(35) Jiao, M.; Li, H.-T.; Chen, J.; Minton, A. P.; Liang, Y. Attractive Protein-Polymer Interactions Markedly Alter the Effect of Macromolecular Crowding on Protein Association Equilibria. *Biophys. J.* **2010**, *99*, 914−23.
(36) Ansari, A.; Jones, C. M.; Henry, E. R.; Hofrichter, J.; Eaton, W. A. The Role of Solent Viscosity in the Dynamics of Protein Conformational Changes. *Science* **1992**, *256*, 1796−1798.
(37) Jas, G. S.; Eaton, W. A.; Hofrichter, J. Effect of Viscosity on the Kinetics of a-Helix and B-Hairpin Formation. *J. Phys. Chem. B* **2001**, *105*, 261−272.
(38) Donnert, G.; Keller, J.; Medda, R.; Andrei, M. A.; Rizzoli, S. O.; Lu, R.; Jahn, R.; Eggeling, C.; Hell, S. W. Macromolecular-Scale Resolution in Biological Fluorescence Microscopy. *Proc. Natl. Acad. Sci. U. S. A.* **2006**, *103*, 11440−11445.
(39) Yeow, E. K. L.; Melnikov, S. M.; Bell, T. D. M.; De Schryver, F. C.; Hofkens, J. Characterizing the Fluorescence Intermittency and Photobleaching Kinetics of Dye Molecules Immobilized on a Glass Surface. *J. Phys. Chem. A* **2006**, *110*, 1726−34.
(40) De Meyer, S. F.; Vandeputte, N.; Pareyn, I.; Petrus, I.; Lenting, P. J.; Chuah, M. K. L.; VandenDriessche, T.; Deckmyn, H.; Vanhoorelbeke, K. Restoration of Plasma von Willebrand Factor Deficiency Is Sufficient to Correct Thrombus Formation after Gene Therapy for Severe von Willebrand Disease. *Arterioscler. Thromb. Vasc. Biol.* **2008**, *28*, 1621−6.
(41) De Meyer, S. F.; Budde, U.; Deckmyn, H.; Vanhoorelbeke, K. In Vivo von Willebrand Factor Size Heterogeneity in Spite of the Clinical Deficiency of ADAMTS-13. *J. Thromb. Haemost.* **2011**, *9*, 2506−8.
(42) Destandau, E.; Lefèvre, J.-P.; Chouai Fakhr Eddine, A.; Desportes, S.; Jullien, M. C.; Hierle, R.; Leray, I.; Valeur, B.; Delaire, J. A. A Novel Microfluidic Flow-Injection Analysis Device with Fluorescence Detection for Cation Sensing. Application to Potassium. *Anal. Bioanal. Chem.* **2007**, *387*, 2627−32.
(43) Santiago, J. G.; Wereley, S. T.; Meinhart, C. D.; Beebe, D. J.; Adrian, R. J. A Particle Image Velocimetry System for Microfluidics. *Exp. Fluids* **1998**, *25*, 316−319.
(44) Zheng, X.; Silber-Li, Z. Measurement of Velocity Profiles in a Rectangular Microchannel with Aspect Ratio A = 0.35. *Exp. Fluids* **2008**, *44*, 951−959.
(45) Tokunaga, M.; Imamoto, N.; Sakata-sogawa, K. Highly Inclined Thin Illumination Enables Clear Single-Molecule Imaging in Cells. *Nat. Methods* **2008**, *5*, 159−161.
(46) Uji-i, H.; Melnikov, S. M.; Deres, A.; Bergamini, G.; De Schryver, F.; Herrmann, A.; Müllen, K.; Enderlein, J.; Hofkens, J. Visualizing Spatial and Temporal Heterogeneity of Single Molecule Rotational Diffusion in a Glassy Polymer by Defocused Wide-Field Imaging. *Polymer* **2006**, *47*, 2511−2518.
(47) Larsson, A.; Carlsson, C.; Jonsson, M.; Albinsson, B. Characterization of the Binding of the Fluorescent Dyes YO and YOYO to DNA by Polarized Light Spectroscopy. *J. Am. Chem. Soc.* **1994**, *116*, 8459−8465.
(48) Cosa, G.; Focsaneanu, K. S.; McLean, J. R.; McNamee, J. P.; Scaiano, J. C. Photophysical Properties of Fluorescent DNA-Dyes Bound to Single- and Double-Stranded DNA in Aqueous Buffered Solution. *Photochem. Photobiol.* **2001**, *73*, 585−99.
(49) Di Carlo, D.; Edd, J.; Humphry, K.; Stone, H.; Toner, M. Particle Segregation and Dynamics in Confined Flows. *Phys. Rev. Lett.* **2009**, *102*, 094503.
(50) Schroeder, C. M.; Teixeira, R. E.; Shaqfeh, E. S. G.; Chu, S. Dynamics of DNA in the Flow-Gradient Plane of Steady Shear Flow: Observations and Simulations. *Macromolecules* **2005**, *38*, 1967−1978.
(51) Smith, D. E. Response of Flexible Polymers to a Sudden Elongational Flow. *Science* **1998**, *281*, 1335−1340.
(52) Singh, I.; Shankaran, H.; Beauharnois, M. E.; Xiao, Z.; Alexandridis, P.; Neelamegham, S. Solution Structure of Human von Willebrand Factor Studied Using Small Angle Neutron Scattering. *J. Biol. Chem.* **2006**, *281*, 38266−75.
(53) Singh, I.; Themistou, E.; Porcar, L.; Neelamegham, S. Fluid Shear Induces Conformation Change in Human Blood Protein von Willebrand Factor in Solution. *Biophys. J.* **2009**, *96*, 2313−20.
(54) Perkins, T. T.; Douglas, E. S.; Chu, S. Single Polymer Dynamics in an Elongational Flow. *Science* **1997**, *276*, 2016−2021.
(55) Schneider, S. W.; Nuschele, S.; Wixforth, A.; Gorzelanny, C.; Alexander-Katz, A.; Netz, R. R.; Schneider, M. F. Shear-Induced Unfolding Triggers Adhesion of von Willebrand Factor Fibers. *Proc. Natl. Acad. Sci. U. S. A.* **2007**, *104*, 7899−7903.